PHYSICAL REVIEW E **91**, 022203 (2015)

# Bonded-cell model for particle fracture

Duc-Hanh Nguyen,[1,2,*] Emilien Azéma,[1,†] Philippe Sornay,[2,‡] and Farhang Radjai[1,3,§]
[1]*Université de Montpellier, CNRS, LMGC, Place Eugène Bataillon, 34095 Montpellier, France*
[2]*CEA, DEN, DEC, SPUA, LCU, F-13108 Saint Paul lez Durance, France*
[3]*MultiScale Material Science for Energy and Environment, UMI 3466 CNRS-MIT, CEE, Massachusetts Institute of Technology, 77 Massachusetts Avenue, Cambridge 02139, USA*
(Received 27 August 2014; published 9 February 2015)

Particle degradation and fracture play an important role in natural granular flows and in many applications of granular materials. We analyze the fracture properties of two-dimensional disklike particles modeled as aggregates of rigid cells bonded along their sides by a cohesive Mohr-Coulomb law and simulated by the contact dynamics method. We show that the compressive strength scales with tensile strength between cells but depends also on the friction coefficient and a parameter describing cell shape distribution. The statistical scatter of compressive strength is well described by the Weibull distribution function with a shape parameter varying from 6 to 10 depending on cell shape distribution. We show that this distribution may be understood in terms of percolating critical intercellular contacts. We propose a random-walk model of critical contacts that leads to particle size dependence of the compressive strength in good agreement with our simulation data.

DOI: 10.1103/PhysRevE.91.022203 PACS number(s): 45.70.−n, 83.80.Fg, 62.20.M−, 82.30.Lp

## I. INTRODUCTION

Particle breakage occurs commonly in natural granular flows and industrial processes involving the transport, handling, and compaction of granular materials. The particle size reduction is often undesirable or uncontrolled, and it is referred to as the attrition process. In contrast, the fragmentation of particles under controlled conditions is used in comminution processes such as the milling of vegetal products or grinding of mineral materials. The evolution of particle size distribution and energy dissipation in such processes depend on many factors such as particle properties (shape, crushability), initial size distribution, loading history, and mobility of the grains during the crushing process [1–9].

Both single-particle crushing and fragmentation process of an assembly of particles subjected to shearing or compaction have been subject to experimental investigations in civil engineering and particle technology [10–22]. The compressive strength of a single particle, its variability, and size dependence are essential for understanding the collective response of a granular material to applied loading. The fracture of a particle inside a granular packing depends on the angular positions of its contact neighbors and the normal and tangential forces exerted by them on the particle. For this reason, there is no general analytical model for the fracture of a single particle. The case of a particle subjected to diametrical compression (also called the Brazilian test) has been more carefully considered in this respect. A detailed analytical model was developed by Tsoungui *et al.* using Weibull statistical flaw size distribution and compared to experiments [23]. Two different fracture modes were analyzed in this model: (1) the volume fracture mode in which a transversal crack responsible of particle fracture originates near the center and propagates towards the contact points and (2) the contact fracture mode characterized by the propagation of cracks initiated at the contact points toward the center of the particles. The experiments performed on a brittle material suggest that the volume fracture mode is more likely to occur in large-enough particles.

Several authors have used the finite element method (FEM) to study single-particle fracture by incorporating the material behavior and an adequate damage or rupture criterion [23–26]. This method has the advantage of accounting for the true nature of the material and provides access to the full stress field in a continuum framework. But it requires rather fine meshing of the particle at its borders or at least around its contact points with other particles and at crack tips. Its application to an assembly of particles further requires a proper treatment of frictional contacts and large deformations, which make it computationally inefficient.

Numerical simulations by the molecular dynamics (MD) method or discrete element method (DEM) have been increasingly employed in order to get a better understanding of the particle-scale mechanisms of the comminution process [1,9,27–31]. Such methods combine the general framework of the DEM, based on rigid-body dynamics and frictional contact interactions, with a particle fracture model. DEM numerical models have the advantage of allowing for the treatment of frictional contact interactions and they provide detailed information about local particle environments and force chains that control the breakup events.

The most straightforward DEM-based approach consists in modeling the particles as aggregates of spherical subparticles bonded together by cohesive forces. Such aggregates may represent real aggregates such as pellets and ceramic compacts or simply be regarded as a toy model for particle fracture. This bonded particle model (BPM) has been employed to investigate the behavior of crushable soils, rocks, fault gouge, and other materials [7,22,32–41]. An alternative method consists in replacing a circular or spherical particle at its fracture threshold by several smaller fragments of the same shape [42–46]. A major issue with

*dhnguyen2015@gmail.com
†emilien.azema@univ-montp2.fr
‡philippe.sornay@cea.fr
§franck.radjai@univ-montp2.fr

 

these methods is that an aggregate of spherical subparticles includes voids, so its breakup leads to considerable loss of volume.

To circumvent the volume-loss issue, several authors have used polygonal or polyhedral subparticles or cells generated by Voronoi tessellation [47–50]. These cells pave the whole volume of the particle so the volume is conserved during particle fracture and fragmentation. Such bonded cell models (BCM) involve extended intercellular contacts that need to be modeled differently from contacts between spherical particles. In previous studies, the cells were interconnected by linear springs with a breaking threshold [49,50]. The representation of intercellular contacts by a linear force law as that between spherical subparticles is, however, an unphysical approximation since the contacts extend along a line [in two dimensions (2D)] or a surface (in 3D) between cells and thus their treatment needs at least two or three displacement variables, respectively. The cracks propagate along these contacts as intergranular cracks in polycrystalline materials.

In this paper, we use the BCM approach with the contact dynamics (CD) method to investigate the fracture properties of disklike particles subjected to diametrical compression [51–53]. Each particle is modeled as an aggregate of perfectly rigid cells with their common sides modeled as frictional-cohesive contacts. The framework of the CD method allows us to account for the perfectly rigid behavior of the cells and the correct kinematics of side-side contacts. Since the cells are treated as perfectly rigid elements, in contrast to linear spring-dashpot models of contact, a crack is generated only when all critical intercellular contacts (contacts at their tensile threshold) percolate across the particle. We are interested in the compressive strength of a single particle under uniaxial compression in this model with focus on its variability and size dependence. Our findings are of potential interest to intergranular fracture in polycristalline materials, rock fracture, and quasibrittle fracture of biomaterials.

In the following, we first describe the numerical model. Then, in Sec. III, we investigate the effects of cell size distribution. Section IV is devoted to the variability of compressive strength. In Sec. V we study size dependence and introduce a simple model based on critical paths. We conclude with a brief discussion of major findings of this work.

## II. BONDED CELL MODEL

Each particle is divided into $n_v$ cells by Voronoi tessellation, as shown in Fig. 1, each cell representing a rigid subparticle. For a particle of area $S$, the number of cells is given by $n_v = S/d_0^2$, where $d_0$ is the average cell size. $n_v$ points are distributed randomly on the surface of the polygon by imposing that the distance $\ell$ between the points is larger than a minimum distance $\ell_{\min} = \lambda d_0$, as shown in the Fig. 1(a). The parameter $\lambda$ represents the degree of regularity of meshing or the span of cell size distribution. Indeed, for $\lambda = 1$ the total surface may be meshed by squares of side $d_0$ for $S/d_0^2$ points. Hence, in order to allow for cells of five sides and more, it is necessary to reduce $\lambda$. Figures 1(b) and 1(c) present two examples of meshing of a circle for $\lambda = 0$ and $\lambda = 0.8$, corresponding to very irregular and regular meshes,

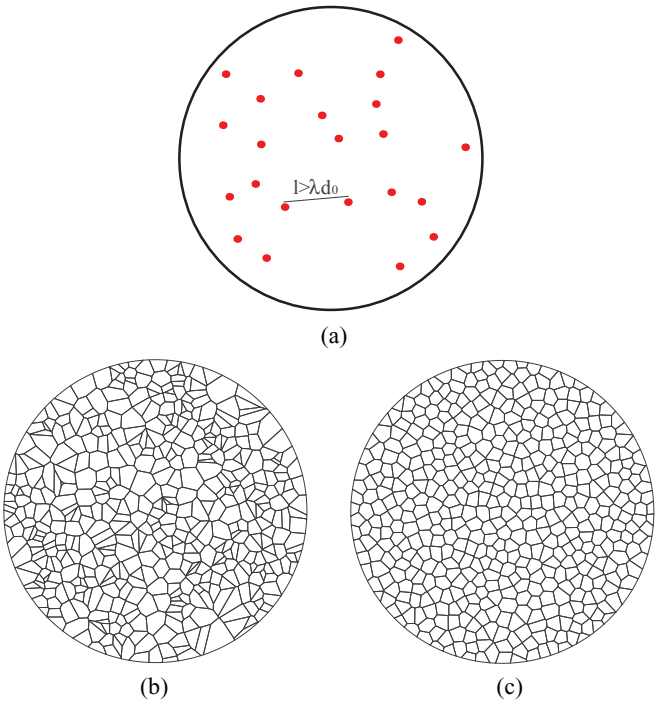


FIG. 1. (Color online) Definition of the degree of regularity of the mesh $\lambda$ (a) and two examples of the discretization for $\lambda = 0$ (b) and $\lambda = 0.8$ (c).

respectively. We will see that $\lambda$ affects the variability of fracture behavior.

A key issue in using DEM with crushable aggregates is the statistical representativity of the particles and their fragments during crushing. In fact, the sizes of the initial aggregates and cells are, respectively, the upper and lower bounds on the size distribution of fragments in the debris. The statistical representivity of particle size distribution in the process of fragmentation is therefore determined by their ratio. Moreover, the mechanical behavior and fracture of a particle depends on the number of cells. At the same time, since the cells are treated as subparticles interacting via cohesion forces, the computation time increases with their number. Hence, it is essential to optimize the number of cells per particle in order to be able to include a large number of particles in the initial configuration of the sample.

The cells are assumed to interact via cohesive frictional contacts along their common sides. A side-side contact between two rigid cells involves two unilateral constraints. In other words, at least two repulsive forces along the common side are necessary to prevent from their overlap. In practice, a side-side contact should therefore be represented by two contact points, as shown in Fig. 2, and the normal direction is the normal to the common side. The cell motions are governed by equations of dynamics and at each side-side contact two forces need to be calculated. The choice of the two contact points representing a side-side contact is matter of convenience. Only the resultant force at each side-side contact and its point of application are physically meaningful and independent of the choice of the positions of contact points.

A side-side contact may open only at one of the two points by pivoting around the other point. It may also open

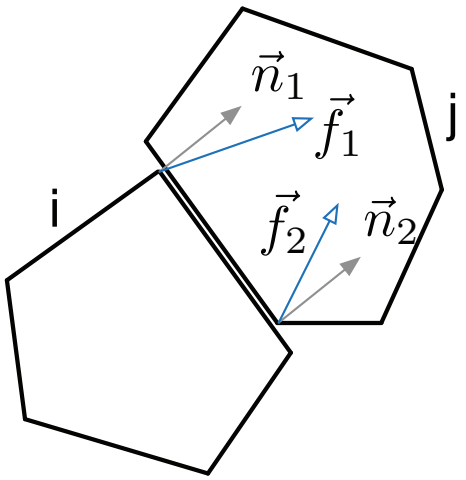


FIG. 2. (Color online) Contact dynamics model of a side-side contact between two particles by two contact points with their normals $\vec{n}_1$ and $\vec{n}_2$ and forces $\vec{f}_1$ and $\vec{f}_2$.

simultaneously at both points. The normal adhesion threshold $f_c$ between two cells linearly depends on the length $L$ of the contact. Since the contact is represented by two points, the tensile threshold is given by $f_c = \sigma_c L/2$, where $\sigma_c$ is the internal cohesion of the material. This means that a side-side contact can lose its cohesion for normal force $f_n = -\sigma_c L/2$ reached at any of the two contact points representing the side-side contact. But if none of the two normal forces $f_{1n}$ and $f_{2n}$ at the two contact points is critical, then they continue to increase with no loss of cohesion and the particles remain glued together until the total normal force $f_{1n} + f_{2n} = 2f_c = L\sigma_c$. This situation is, however, very rare since the particles are most of time subjected to force moments so the total torque $(f_{1n} - f_{2n})L \neq 0$ and thus a side-side contact opens mainly when $f_c$ is reached at only one of the two contact points.

The shear strength along a side-side contact is given by $\tau_c = \mu_s \sigma_c$, where $\mu_s$ is the internal friction coefficient. A side-side contact may lose its cohesion only when the total tangential force $f_{1t} + f_{2t}$ at the two contact points representing the side-side contact reaches the sliding threshold $\mu_s(f_{1n} + f_{2n} + 2f_c)$. The choice of a frictional material behavior is not mandatory and $\tau_c$ may be defined independently of $\sigma_c$. In order to limit the number of independent parameters, in this paper we used a Coulomb friction law. But the effect of local cracking criterion may be a subject of detailed investigation in the BCM framework.

When the cohesion between two cells is lost along a side-side contact, the latter turns into a crack governed by frictional contact behavior. The loss of cohesion is assumed to be irreversible. The cohesive state between cells is managed by a matrix $M$. $M[i,j] = 1$ if the cells $i$ and $j$ are connected by a cohesive contact. Otherwise, we set $M[i,j] = 0$. This matrix is updated at each time step according to the evolution of the contacts.

The simulations were carried out by means of the CD method, which is suitable for simulating large assemblies of undeformable particles [51–54]. In this method, the rigid-body equations of motion are integrated by taking into account the kinematic constraints resulting from contact interactions. These interactions are characterized by three parameters: the coefficient of friction and the coefficients of normal and tangential restitution that control the rate of dissipation. An implicit time-stepping scheme makes the method unconditionally stable. In contrast to the molecular dynamics method, in the CD method tiny overlaps between particles are used for contact detection but they do not represent an elastic deflection. For this reason, the time step can be larger than that in the molecular dynamics method. In CD, an iterative algorithm based on nonlinear Gauss-Seidel iterations is used to determine the contact forces and particle velocities simultaneously at all potential contacts. The CD method has been extensively employed for the simulation of granular materials in 2D and 3D [55–72].

The CD method is based on implicit time integration of velocities but requires an explicit determination of the contact network at the beginning of each time step [52,73]. The contact detection between two bodies consists in looking the portions of space they occupy. The treatment of the mechanical interaction requires additionally the identification of a common tangent plane (a line in 2D). Of course, contacts may take place through a larger contact zone than a single point. In 2D simulations of the present paper, the detection of contact between two convex polygonal bodies was implemented through the so-called shadow overlap method [73,74].

## III. BOUNDARY CONDITIONS

In this paper, we use the BCM to study the breakup of a single circular particle crushed between two platens. This "Brazilian" test will be used to investigate the effects of model parameters $\sigma_c$, $\mu_s$, $\lambda$, and $n_v$. The particle is crushed by applying stepwise displacements $\delta_y$ to the top and bottom platens. The total axial strain after $N$ steps is given by $N\delta_y/d$, where $d$ is particle diameter. Let $F$ be the axial force exerted on the particle; see Fig. 3. The average vertical stress $\sigma_a$ acting on the particle is given by

$$\sigma_a = \langle \sigma_{yy} \rangle = \frac{F}{d}. \tag{1}$$

We calculate $\sigma_a$ directly from the forces between cells [75]:

$$\langle \sigma_{yy} \rangle = n_c \langle f_y \ell_y \rangle, \tag{2}$$

where $n_c$ is the number density of contacts, $f_y$ is the $y$ component of the reaction force between two particles, and

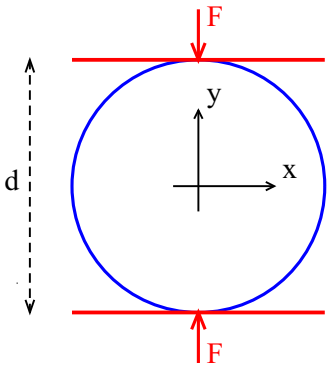


FIG. 3. (Color online) Boundary conditions for Brazilian crushing of a particle.

$\ell_y$ is the $y$ component of the branch vector joining their centers. The averaging runs over all intercell contacts inside the particle. The average horizontal stress $\langle\sigma_{xx}\rangle$ is zero. We note that since the particle is rigid, in principle, no axial deformation must occur until the particle breaks. But some deformation does occur numerically without causing fracture. Such deformations are small and do not affect the stress values, which are determined by contact dynamics calculations. Video samples of the simulations analyzed below can be found by following the link www.cgp-gateway.org/ref032.

## IV. FRACTURE CHARACTERISTICS

Figure 4 displays snapshots of a cell-meshed particle at incipient cracking together with compressive and tensile forces between cells for two different values of cell-shape variability parameter λ. The main crack is nearly vertical and corresponds on average to a mode I fracture as observed in experiments [76]. However, deviations from the vertical and zigzag aspect of the main crack, which reflect the coarse meshing of the particle, indicate that cellular disorder and friction forces between cells are important for the fracture. We also observe secondary cracks and small fragments detached from the particle.

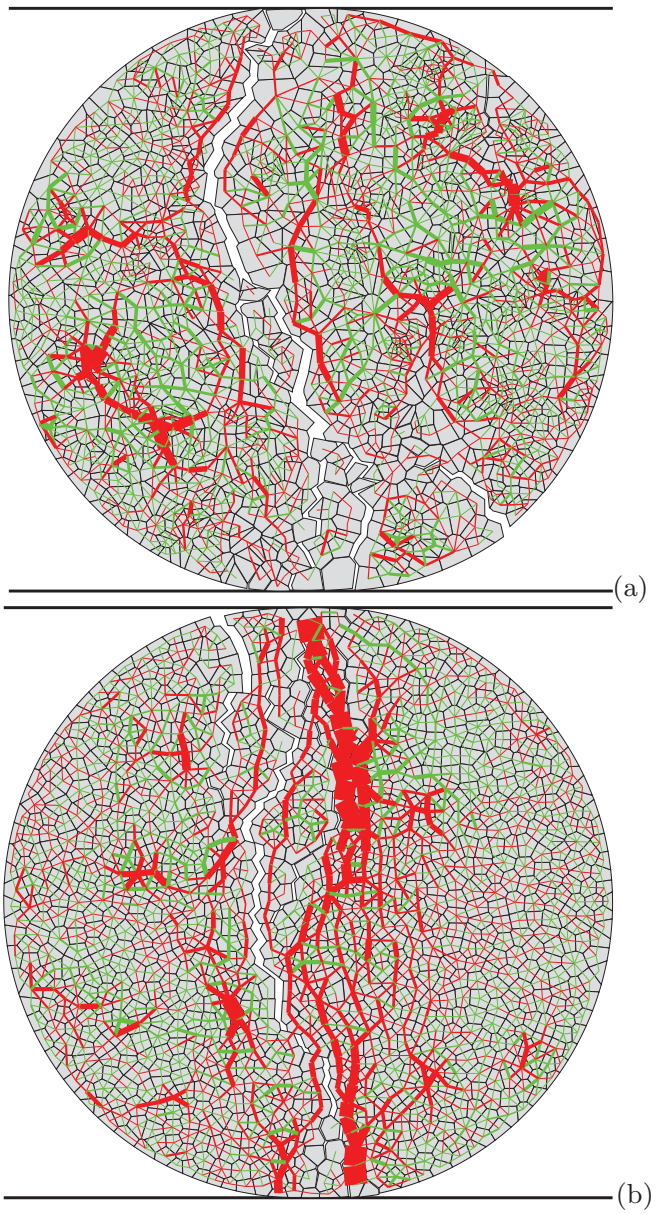


FIG. 4. (Color online) A single circular particle subjected to diametral compression (Brazilian test) for $\lambda = 0$ (a) and $\lambda = 0.8$ (b). The red and green lines represent compressive and tensile contacts, respectively.

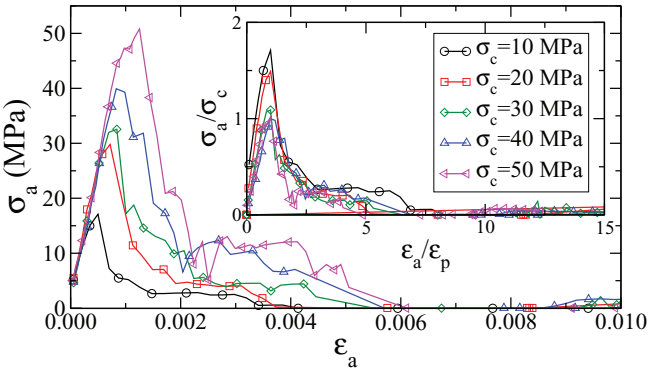


FIG. 5. (Color online) Axial stress versus axial strain for several values of tensile strength $\sigma_c$. The inset shows the axial stress normalized by $\sigma_c$. The parameters are $\mu_s = 0.3$, $\lambda = 0.8$, and $n_v = 50$.

Figure 5 shows axial stress $\sigma_a$ as a function of axial deformation $\varepsilon_a$ for different values of tensile strength $\sigma_c$. The stress sharply increases with strain and falls off abruptly when fracture is triggered. The stress peak $\sigma_p$ is the compressive strength of the particle. Except for the lowest values of cohesion, it scales with $\sigma_c$, as shown in the inset. The higher value of $\sigma_p/\sigma_c$ in the low-cohesion limit indicates that the compressive strength is determined by both the tensile strength (normal strength) and shear strength, which is enhanced by interlocking between cells.

In order to quantify the influence of local friction coefficient $\mu_s$, a series of crushing tests were conducted with 11 values of $\mu_s$ from 0 to 1 with all other parameters kept at a fixed value ($\sigma_c = 10$ MPa, $\lambda = 0.8$, and $n_v = 500$). For each value of $\mu_s$, nine simulations with independent tessellations were performed. Figure 6 shows the evolution of the average compressive strength $\sigma_p$ (peak stress) normalized by $\sigma_c$ as a function of $\mu_s$. We see that, as expected, the compressive strength increases with friction coefficient. Its dependence with respect to the friction coefficient is, however, rather weak since it increases from $0.4\sigma_c$ to $1.2\sigma_c$ as $\mu_s$ is increased from 0 to 1. This weak dependence may be attributed to the fact that in Brazilian test the rupture occurs in tension. But the effect of friction coefficient clearly shows that the mobilization of friction forces along the crack path is an important factor for compressive strength.

## V. STRENGTH VARIABILITY

Another issue that we would like to address here is the statistical scatter of compressive strength and its possible scale dependence. Such a scatter may be a consequence of the BCM.

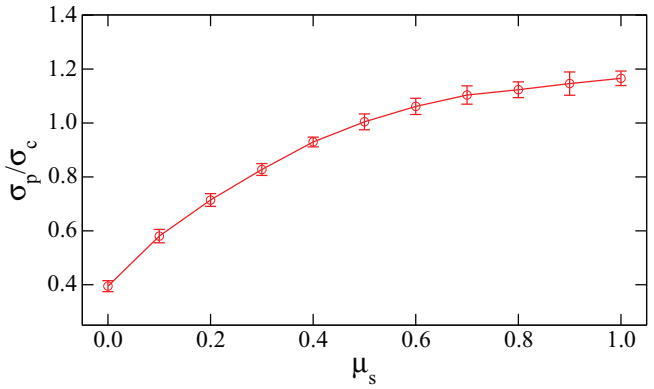


FIG. 6. (Color online) Evolution of compressive strength $\sigma_p$ as a function of local friction coefficient $\mu_s$ for $\sigma_c = 10$ MPa, $\lambda = 0.8$, and $n_v = 500$. The error bars represent standard deviation calculated from nine independent simulations with different tessellations.

In particular, it is important to assess the role of cell shape distribution parameter $\lambda$. To clarify this point, we carried out a series of Brazilian tests for five values of $\lambda$ in the range [0,0.8] with $\sigma_c = 10$ MPa, $\mu_s = 0.3$, and $n_v = 1000$. For each value of $\lambda$, 30 simulations with independent tessellations were performed, allowing us to obtain the variability of the compressive strength, expressed as cumulative survival probability $P_s$ of the particle as a function of $\sigma_a$. This is the probability that the particle does not fail for all stresses below $\sigma_a$.

Figure 7(a) shows the cumulative survival probability $P_s$ in log-log scale as a function of the compressive stress $\sigma_a$ for $\lambda = 0$ and $\lambda = 0.8$. Despite fluctuations, the data are correctly fitted by the cumulative Weibull function [77,78],

$$P_s(\sigma_a) = e^{-(\sigma_a/\sigma_w)^m}, \tag{3}$$

where $\sigma_w$ is a stress scale and $m$ is the Weibull modulus (or shape factor). Both parameters can be extracted from the data. Figure 7(b) shows that $m$ is $\simeq$6 at low values of $\lambda$ and increases up to $\simeq$10 for the largest values of $\lambda$. It is remarkable that this range of values of $m$ corresponds to the observed values in soils and powders although our system is purely 2D [78]. The increase of $m$ indicates lower strength variability consistently with lower cell variability as $\lambda$ increases.

We also note that the compressive strength $\sigma_p$ and scale stress $\sigma_w$ increase with $\lambda$ as observed in Fig. 7(c). For Weibull distribution, it can be shown that $\sigma_p$ and $\sigma_w$ obey the simple relation

$$\sigma_p = \sigma_w \Gamma\left(1 + \frac{1}{m}\right), \tag{4}$$

where $\Gamma$ is the gamma function. This relation is in excellent agreement with our data in Fig. 7(c). Let us remark that the overall Weibull fit to the simulation data reveals also fluctuations in the form of modes as observed in Fig. 7(a). Such deviations indicate that the survival probability reflects not only the overall disorder but also some fine details of the microstructure.

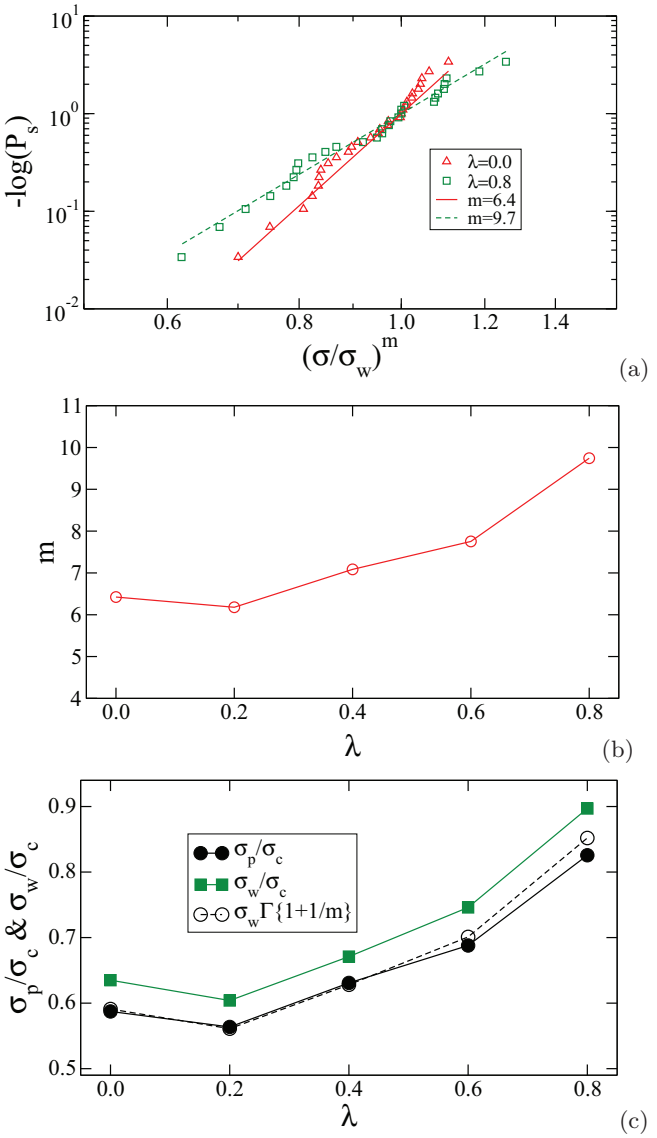


FIG. 7. (Color online) (a) Survival probability of a particle as a function of compressive stress $\sigma_a$ in a Brazilian test for $n_v = 500$ and two values of mesh regularity parameter $\lambda$ in log-log scale. The lines represent fits to the Weibull function with two different values of the Weibull modulus $m$. (b) The Weilbull modulus $m$ as function of $\lambda$. (c) Compressive strength $\sigma_p$ and scale stress $\sigma_w$ as a function of $\lambda$. The open symbols are predicted values of $\sigma_p$ by Eq. (4).

## VI. SCALE DEPENDENCE

The Weibull statistics for brittle materials is generally explained by the distribution of microcracks, which concentrate stresses in the bulk of the material [79]. Their density determines the cracking state and leads to size dependence of the strength [77]:

$$\sigma_p = \sigma_p' \left(\frac{V}{V'}\right)^{-1/m}, \tag{5}$$

where $\sigma_p$ and $\sigma_p'$ are the strength for samples of volumes $V$ and $V'$, respectively. The applicability of this distribution to quasibrittle materials has been questioned by some

authors and deviations from the Weibull statistics have been observed [80–83].

Strictly speaking, there are no cracks in our system, and stress concentration is a consequence of cell-induced disorder. In this respect, the fracture is analogous to intergranular failure in polycrystalline materials. Another feature, which makes our system specific, is that the cells are perfectly rigid and thus their displacements are subject to compatibility with steric exclusions between cells. Hence, when the tensile threshold $-\sigma_c$ is reached at a contact between two cells, it will generally not open unless collectively with other contacts. Since the force at such a *critical* contact cannot exceed its tensile threshold, new force increments are redistributed to neighboring contacts. The loading of the contacts gets therefore accelerated every time a new contact becomes critical. This stress redistribution continues until the critical contacts percolate across the particle, in which case a crack occurs in the sense that all critical contacts open at the same time. Hence, the fracture mode differs from both volume fracture and contact fracture modes described in Ref. [23]. In the simulations, as described in Sec. II, the force at a critical contact is $f_c = -\sigma_c L/2$. The tensile threshold $\sigma_c$ being the same for all contacts, the weakest contact is the one having shortest length $L$. However, the above loading process of contacts implies that the cracking of the particle is not controlled by the weakest contact but requires, on the contrary, the strongest contact (with the longest length) to become critical on the path of a potential crack. Otherwise, none of the critical contacts can open due to kinematic incompatibility. This situation radically contrasts with the assumption of weakest link [84]. Nevertheless, the above argument also indicates that the "flaws" in our system are equivalent to potential crack paths rather than single critical contacts between cells. In other words, considering only the lengths of the contacts, the weakest "link" in our system is the path of intercell contacts having the shortest length. In this sense, the variability of compressive strength reflects the statistics of all paths (with their different lengths and directions), on one hand, and the heterogeneous distribution of forces, as generally observed in granular materials, on the other hand [56,69,85,86].

The statistics of critical contacts and crack paths in our system may naturally lead to size effect but its description cannot be based on the elasticity of the material. Here we introduce a simple model and compare the results with those of Ref. [23]. The number of potential paths of critical contacts increases with the number $n_v \propto (d/d_0)^2$ of cells as a result of either the increase of particle diameter $d$ for a constant cell size $d_0$ or the decrease of $d_0$ for a given particle diameter $d$. In the continuum-mechanics limit, one expects the particle to fracture into two equal fragments along its diameter. In the presence of the cells, the crack follows a more complex path around this mean orientation imposed by the correlations, but the fluctuations around the mean may well be assumed to result from a stochastic process reflecting disorder. Let us assume that the cracks are random walks of equal length $d_0$ from the top and bottom poles towards the center of the particle. Then the mean path is a straight line joining the poles and the standard deviation from this line at the center of the particle varies as $\delta_x \propto n_s^{\alpha}$, where $n_s$ is the number of steps. For a normal random walk we have $\alpha = 1/2$. But the exponent $\alpha$ may take a different value depending on the nature of the network. The number of steps from the poles to the center is simply proportional to $n_v^{1/2}$, so $\delta_x \propto d_0 n_v^{\alpha/2}$. This length may be interpreted as the width of the zone at the center of the disk in which the stresses are concentrated, as illustrated in Fig. 8. Hence, the compressive stress at the center of the particle is $\propto F/\delta_x \propto \sigma_a d/n_v^{\alpha/2} \propto \sigma_a n_v^{(1-\alpha)/2}$.

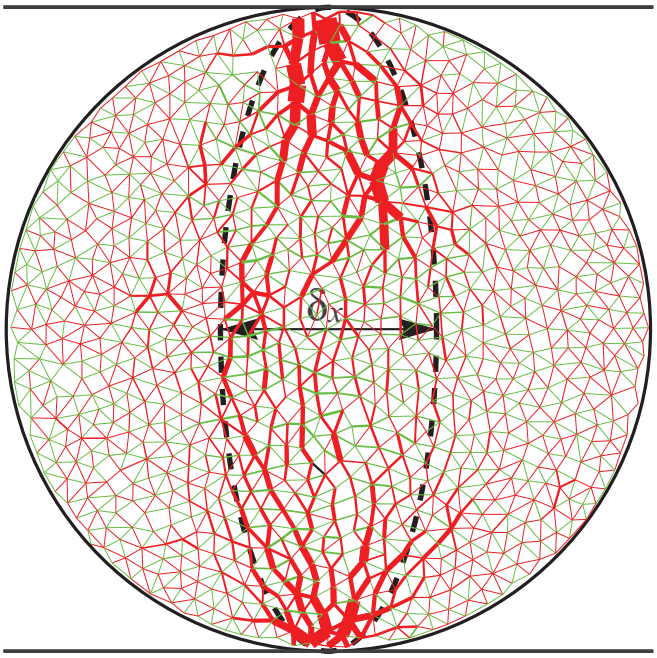


FIG. 8. (Color online) Normal force network before rupture. The dashed lines represent the contours of the stress concentration zone.

The intercellular forces are actually larger in the vicinity of the poles and one might expect failure to be initiated at the poles. But, as argued above, the crack is not effective as long as the cohesion threshold is not reached inside the whole range defined by the random walk. Hence, in this "traction zone," failure occurs when the weakest compressive stress becomes critical. The weakest compressive stress occurs in the center where the compressive forces are dispersed. This stress with $\sigma_a = \sigma_p$ is balanced by a tensile stress equal to $\sigma_c$ in the $y$ direction, so $F/\delta_x \propto \sigma_c$, thereby

$$\frac{\sigma_p}{\sigma_c} \propto n_v^{-(1-\alpha)/2} \propto d^{-(1-\alpha)}. \tag{6}$$

This model predicts a size dependence with exponent $-(1-\alpha)$.

Figure 9(a) shows $\sigma_p$ as a function of $n_v$ for $\lambda = 0.8$ and 16 different combinations of the values of $d$ and $d_0$ with 11 independent tests for each combination. Within our statistical precision, we observe a power law $\sigma_p \propto \sigma_c\ n_v^{-b}$ with $b \simeq 0.24$. This yields $\alpha \simeq 1/2$, which corresponds to a normal random walk. The scale stress $\sigma_w$ follows the same behavior as a function of $n_v$. Figure 9(b) shows $\sigma_p$ as a function of $n_v$ for $\lambda = 0$ and $\lambda = 0.8$. The exponent for $\lambda = 0$ is $b \simeq 0.3$, which corresponds to $\alpha \simeq 0.4$. This "subdiffusive" feature of crack paths may simply be attributed to the fact that, for $\lambda = 0$, there is no constraint on the cell sizes and their shapes so the critical contacts are more likely to occur in more complex

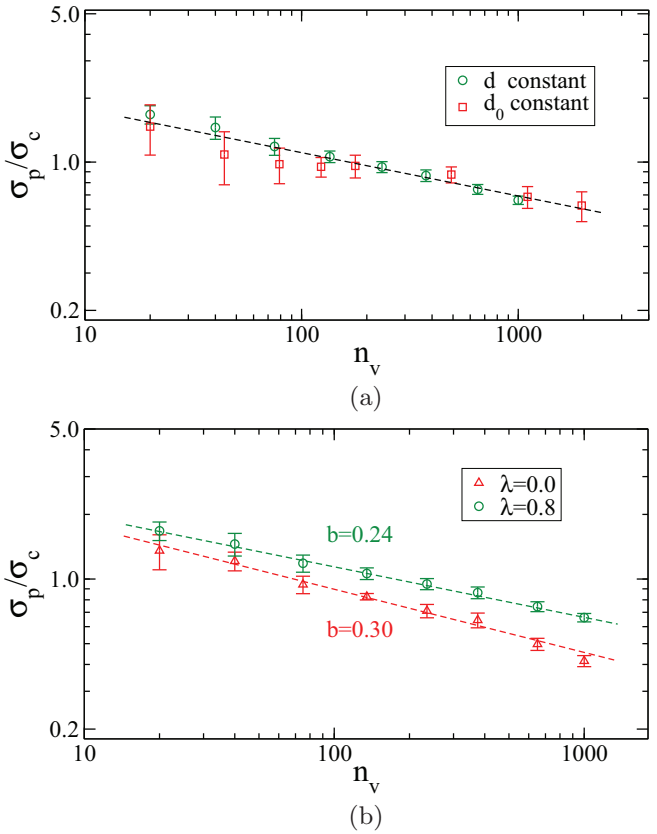


FIG. 9. (Color online) (a) Compressive strength of a particle normalized by internal cohesion as a function of the number of cells for constant particle diameter $d$ and varying cell size $d_0$ (green circle) and for constant $d_0$ and varying $d$ (red square). The error bars represent standard variation for 11 independent simulations. (b) Compressive strength as a function of the number of cells for two extreme values of mesh variability parameter $\lambda$.

configurations. The exponent predicted by elastic theory is $b = 1 - 2/m$ for volume fracture [23]. This implies $1 - \alpha = 2/m$, which is consistent for $\lambda = 0$ and $\lambda = 0.8$ for which we have $m \simeq 6$ and $m \simeq 10$, thus yielding $1 - \alpha \simeq 1/3$ and $1 - \alpha \simeq 1/5$, respectively.

These observations show clearly that the fracture of cell-structured materials is scale dependent. The model based on crack-path statistics around the mean, as briefly outlined above, provides quantitative prediction of the exponent. What is more, it generalizes the weakest-link assumption to the more general "weakest-path" mechanism governed by the percolation of critical contacts. Size effect in single-particle fracture suggests that in an assembly of crushable particles the largest particles are most susceptible to break. However, particle size affects the local distribution of contact forces. In particular, large particles have more contacts and sustain for this reason lower deviatoric stresses. Due to such competing effects, the fragmentation of a granular packing is a complex process.

## VII. CONCLUSION

In this paper, we introduced a BCM in the framework of the contact dynamics method for the investigation of fracture strength properties of circular particles subjected to axial compression. The particles are modeled as aggregates of polygonal rigid cells bonded by the action of cohesion forces along their common sides. Our approach allows for both the conservation of volume and rigorous treatment of unilateral constraints at intercellular contacts.

The compressive strength was shown to scale well with tensile threshold between cells. However, due to the Mohr-Coulomb plastic criterion and interlocking between rigid cells, the strength is also an increasing function of the friction coefficient. By means of extensive simulations, we also performed a detailed parametric analysis of strength variability. The statistical scatter of the data is well described by the Weibull distribution function. This distribution provides a good fit to our data independently of cell shape distribution but the Weibull modulus varies from 6 to 10 as the cell shape span is reduced.

The Weibull distribution of the data in our system was discussed and modeled in terms of critical intercellular contacts and their percolation across the particle. The fracture is controlled by the population of weakest paths from the force application point to the center of the particle. Assuming that those paths are composed of random walks through intergranular contacts, they define a stress concentration zone with a high density of critical contacts. This leads to a power-law particle size dependence of the compressive strength, in close agreement with our simulation data. The value of the exponent in the case of nearly regular cells is consistent with a normal random-walk feature of the crack, whereas for irregular cells it is anomalous.

The Brazilian compression test is often used for indirect measurement of tensile strength in brittle materials [87,88]. But the tensile strength measured from diametral compression tests are usually lower compared to other uniaxial tests. In contrast to theoretical prediction, the cracks do not always propagate from the center to the periphery of the sample as a result of surface defects, which lead to failure by shearing at the contact points with platens. Our simulations are consistent with this picture although the cells are rigid and the crack opens only when critical contacts percolate across the particle. For this reason, we also have a good scaling of the compressive strength with internal cohesion.

A detailed description of single-particle fracture in this paper was made possible by extensive 2D simulations. It is straightforward to extend this work to investigate the role of the contact law such as non-Coulomb friction and damage for the scaling of compressive strength. Another possible extension is the fracture of noncircular particles. We applied the BCM approach to the fragmentation of an assembly of polygonal particles. Our simulations reproduce correctly and efficiently the nonlinear and inhomogeneous features of the comminution process such as the shattering instability and survival of many large particles. Size effect in single-particle fracture suggests that in an assembly of crushable particles the largest particles are most susceptible to breakage. However, particle size affects the local distribution of contact forces. In particular, large particles have more contacts and for this reason sustain lower deviatoric stresses. The results of this work will be reported elsewhere.

[1] C. Thornton, K. K. Yin, and M. J. Adams, J. Phys. D: Appl. Phys. **29**, 424 (1996).
[2] D. Fuerstenau, O. Gutsche, and P. Kapur, in *Comminution 1994*, edited by K. Forssberg and K. Schönert (Elsevier, Amsterdam, 1996), pp. 521–537.
[3] C. Couroyer, Z. Ning, and M. Ghadiri, Powder Technol. **109**, 241 (2000).
[4] A. V. Potapov and C. S. Campbell, Powder Technol. **120**, 164 (2001).
[5] Y. Nakata, M. Hyodo, A. F. Hyde, Y. Kato, and H. Murata, Soils Found. **41**, 69 (2001).
[6] P. Cleary, Miner. Eng. **14**, 1295 (2001).
[7] M. D. Bolton, Y. Nakota, and Y. P. Cheng, Géotechnique **58**, 471 (2008).
[8] C. Hosten and H. Cimilli, Int. J. Miner. Process. **91**, 81 (2009).
[9] L. Liu, K. Kafui, and C. Thornton, Powder Technol. **199**, 189 (2010).
[10] J. Jaeger, in *International Journal of Rock Mechanics and Mining Sciences & Geomechanics Abstracts* (Elsevier, Amsterdam, 1967), Vol. 4, pp. 219–227.
[11] K. L. Lee and I. Farhoomand, Can. Geotech. J. **4**, 68 (1967).
[12] B. O. Hardin, J. Geotech. Eng. **111**, 1177 (1985).
[13] M. Hagerty, D. Hite, C. Ullrich, and D. Hagerty, J. Geotech. Eng. **119**, 1 (1993).
[14] M. Eriksson and G. Alderborn, Pharm. Res. **12**, 1031 (1995).
[15] P. V. Lade, J. A. Yamamuro, and P. A. Bopp, J. Geotech. Eng. **122**, 309 (1996).
[16] M. R. Coop, K. K. Sorensen, T. B. Freitas, and G. Georgoutsos, Géotechnique **54**, 157 (2004).
[17] H. Arslan, G. Baykal, and S. Sture, Granul. Matter **11**, 87 (2009).
[18] B. Imre, J. Laue, and S. M. Springman, Granul. Matter **12**, 267 (2010).
[19] V. Bandini and M. R. COOP, Soils Found. **51**, 591 (2011).
[20] A. Ezaoui, T. Lecompte, H. Di Benedetto, and E. Garcia, Granul. Matter **13**, 283 (2011).
[21] F. Casini, G. M. Viggiani, and S. M. Springman, Granul. Matter **15**, 661 (2013).
[22] J. Huang, S. Xu, and S. Hu, Mech. Mater. **68**, 15 (2014).
[23] O. Tsoungui, D. Vallet, J. Charmet, and S. Roux, Granul. Matter **2**, 19 (1999).
[24] H. Liu, S. Kou, and P.-A. Lindqvist, Mech. Mater. **37**, 935 (2005).
[25] W. Schubert, M. Khanal, and J. Tomas, Int. J. Miner. Process. **75**, 41 (2005).
[26] A. Bäckström, J. Antikainen, T. Backers, X. Feng, L. Jing, A. Kobayashi, T. Koyama, P. Pan, M. Rinne, B. Shen *et al.*, Int. J. Rock Mech. Min. Sci. **45**, 1126 (2008).
[27] R. Moreno, M. Ghadiri, and S. Antony, Powder Technol. **130**, 132 (2003).
[28] S. Antonyuk, M. Khanal, J. Tomas, S. Heinrich, and L. Mörl, Chem. Eng. Process. **45**, 838 (2006).
[29] F. Wittel, H. Carmona, F. Kun, and H. Herrmann, Int. J. Fract. **154**, 105 (2008).
[30] J. Wang and H. Yan, Int. J. Numer. Anal. Methods Geomech. **37**, 832 (2013).
[31] G. Ma, W. Zhou, and X.-L. Chang, Comput. Geotech. **61**, 132 (2014).
[32] Y. Cheng, Y. Nakata, and M. Bolton, Geotechnique **53**, 633 (2003).
[33] D. Potyondy and P. Cundall, Int. J. Rock Mech. Min. Sci. **41**, 1329 (2004).
[34] Y. P. Cheng, M. D. Bolton, and Y. Nakata, Géotechnique **54**, 131 (2004).
[35] N. Cho, C. Martin, and D. Sego, Int. J. Rock Mech. Min. Sci. **44**, 997 (2007).
[36] M. Khanal, W. Schubert, and J. Tomas, Miner. Engin. **20**, 179 (2007).
[37] S. Abe and K. Mair, Geophys. Res. Lett. **36**, L23302 (2009).
[38] J. Wang and H. Yan, Soils Found. **52**, 644 (2012).
[39] G. Timár, F. Kun, H. A. Carmona, and H. J. Herrmann, Phys. Rev. E **86**, 016113 (2012).
[40] M. J. Metzger and B. J. Glasser, Powder Technol. **217**, 304 (2012).
[41] T. Ueda, T. Matsushima, and Y. Yamada, Granul. Matter **15**, 675 (2013).
[42] J. Astrom and H. Herrmann, Eur. Phys. J. B **5**, 551 (1998).
[43] O. Tsoungui, D. Vallet, and J. Charmet, Powder Technol. **105**, 190 (1999).
[44] O. Ben-Nun, I. Einav, and A. Tordesillas, Phys. Rev. Lett. **104**, 108001 (2010).
[45] L. Elghezal, M. Jamei, and I.-O. Georgopoulos, Granul. Matter **15**, 685 (2013).
[46] V. Esnault and J.-N. Roux, Mech. Mater. **66**, 88 (2013).
[47] F. Kun and H. J. Herrmann, Comput. Methods Appl. Mech. Eng. **138**, 3 (1996).
[48] B. Van de Steen, A. Vervoort, and J. Napier, Int. J. Fract. **108**, 165 (2001).
[49] G. D'Addetta, F. Kun, and E. Ramm, Granul. Matter **4**, 77 (2002).
[50] S. Galindo-Torres, D. Pedroso, D. Williams, and L. Li, Comput. Phys. Commun. **183**, 266 (2012).
[51] J. Moreau, European J. Mech. A Solids **13**, 93 (1994).
[52] F. Radjaï and V. Richefeu, Mech. Mater. **41**, 715 (2009).
[53] F. Radjaï and F. Dubois, *Discrete Numerical Modeling of Granular Materials* (Wiley-ISTE, New York, 2011).
[54] M. Jean, Comput. Methods Appl. Mech. Eng. **177**, 235 (1999).
[55] J. Moreau, Eur. J. Mech. A Solids Supp. **13**, 93 (1994).
[56] F. Radjai, M. Jean, J.-J. Moreau, and S. Roux, Phys. Rev. Lett. **77**, 274 (1996).
[57] L. Staron, J.-P. Vilotte, and F. Radjai, Phys. Rev. Lett. **89**, 204302 (2002).
[58] A. Taboada, K. J. Chang, F. Radjaï, and F. Bouchette, J. Geophys. Res. **110**, 1 (2005).
[59] M. Renouf and P. Alart, Comput. Methods Appl. Mech. Eng. **194**, 2019 (2005).
[60] E. Azéma, F. Radjaï, R. Peyroux, F. Dubois, and G. Saussine, Phys. Rev. E **74**, 031302 (2006).
[61] E. Azéma, F. Radjaï, R. Peyroux, V. Richefeu, and G. Saussine, Eur. Phys. J. E **26**, 327 (2008).
[62] N. Estrada, A. Taboada, and F. Radjaï, Phys. Rev. E **78**, 021301 (2008).
[63] E. Azéma and F. Radjaï, Phys. Rev. E **81**, 051304 (2010).
[64] E. Azéma and F. Radjaï, Phys. Rev. E **85**, 031303 (2012).
[65] N. Estrada, E. Azéma, F. Radjai, and A. Taboada, Phys. Rev. E **84**, 011306 (2011).
[66] V. Visseq, A. Martin, D. Iceta, E. Azéma, D. Dureisseix, and P. Alart, Comput. Mech. **49**, 709 (2012).
[67] B. Saint-Cyr, J.-Y. Delenne, C. Voivret, F. Radjai, and P. Sornay, Phys. Rev. E **84**, 041302 (2011).

[68] J. C. Quezada, P. Breul, G. Saussine, and F. Radjai, Phys. Rev. E **86**, 031308 (2012).
[69] C. Voivret, F. Radjaï, J.-Y. Delenne, and M. S. El Youssoufi, Phys. Rev. Lett. **102**, 178001 (2009).
[70] D. Kadau, G. Bartels, L. Brendel, and D. E. Wolf, Comput. Phys. Commun. **147**, 190 (2002).
[71] I. Bratberg, F. Radjai, and A. Hansen, Phys. Rev. E **66**, 031303 (2002).
[72] D.-H. Nguyen, E. Azéma, F. Radjai, and P. Sornay, Phys. Rev. E **90**, 012202 (2014).
[73] E. Azéma, N. Estrada, and F. Radjaï, Phys. Rev. E **86**, 041301 (2012).
[74] G. Saussine, C. Cholet, P. Gautier, F. Dubois, C. Bohatier, and J. Moreau, Comput. Methods Appl. Mech. Eng. **195**, 2841 (2006).
[75] L. Staron, F. Radjaï, and J.-P. Vilotte, Eur. Phys. J. E **18**, 311 (2005).
[76] K. Schönert, Powder Technol. **143-144**, 2 (2004).
[77] W. Weibull, J. Appl. Mech. **18**, 293 (1951).
[78] G. R. McDowell and M. D. Bolton, Géotechnique **48**, 667 (1998).
[79] A. A. Griffith, Phil. Trans. Roy. Soc. **221**, 163 (1920).
[80] S. van der Zwaag, ASTM J. Test. Eval. **17**, 292 (1989).
[81] X. Gao, R. Dodds, R. Tregoning, J. Joyce, and R. Link, Fatigue Fract. Eng. Mater. Struct. **22**, 481 (1999).
[82] Y. Nakata, Y. Kato, M. Hyodo, A. F. HYDE, and H. Murata, Soils Found. **41**, 39 (2001).
[83] Z. Bertalan, A. Shekhawat, J. P. Sethna, and S. Zapperi, Phys. Rev. Appl. **2**, 034008 (2014).
[84] S. Batdorf and H. Heinisch, J. Am. Ceram. Soc. **61**, 355 (1978).
[85] R. P. Behringer, K. E. Daniels, T. S. Majmudar, and M. Sperl, R. Soc. A **366**, 493 (2008).
[86] V. Richefeu, Moulay Saïd El Youssoufi, and F. Radjaï, Phys. Rev. E **73**, 051304 (2006).
[87] M. K. Fahad, J. Mater. Sci. **31**, 3723 (1996).
[88] A. T. Procopio, A. Zavaliangos, and J. C. Cunningham, J. Mater. Sci. **38**, 3629 (2003).